Simulation of very severe cyclone Mala over Bay of Bengal with HWRF modeling system

Sujata Pattanayak, U. C. Mohanty & S. G. Gopalakrishnan

Natural Hazards
Journal of the International Society for the Prevention and Mitigation of Natural Hazards

ISSN 0921-030X

Nat Hazards
DOI 10.1007/s11069-011-9863-z

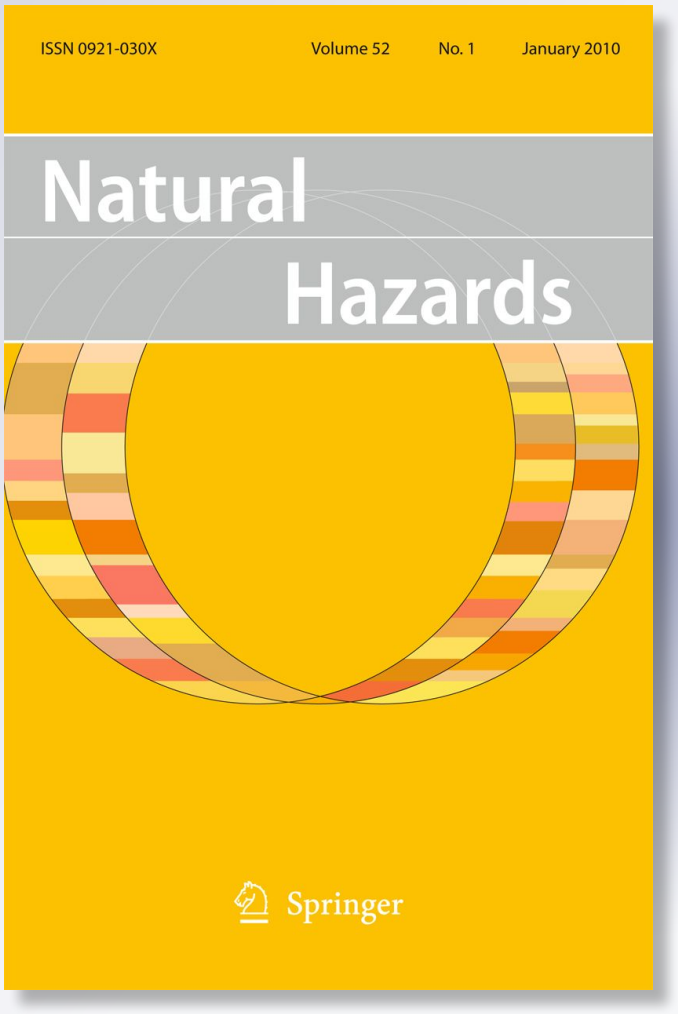

Springer

Nat Hazards
DOI 10.1007/s11069-011-9863-z

ORIGINAL PAPER

Simulation of very severe cyclone Mala over Bay of Bengal with HWRF modeling system

Sujata Pattanayak · U. C. Mohanty · S. G. Gopalakrishnan

Received: 19 November 2010 / Accepted: 19 May 2011

Abstract Tropical cyclone is one of the most devastating weather phenomena all over the world. The Environmental Modeling Center (EMC) of the National Center for Environmental Prediction (NCEP) has developed a sophisticated mesoscale model known as Hurricane Weather Research and Forecasting (HWRF) system for tropical cyclone studies. The state-of-the-art HWRF model (atmospheric component) has been used in simulating most of the features our present study of a very severe tropical cyclone "Mala", which developed on April 26 over the Bay of Bengal and crossed the Arakan coast of Myanmar on April 29, 2006. The initial and lateral boundary conditions are obtained from Global Forecast System (GFS) analysis and forecast fields of the NCEP, respectively. The performance of the model is evaluated with simulation of cyclone Mala with six different initial conditions at an interval of 12 h each from 00 UTC 25 April 2006 to 12 UTC 27 April 2006. The best result in terms of track and intensity forecast as obtained from different initial conditions is further investigated for large-scale fields and structure of the cyclone. For this purpose, a number of important predicted fields' viz. central pressure/pressure drop, winds, precipitation, etc. are verified against observations/verification analysis. Also, some of the simulated diagnostic fields such as relative vorticity, pressure vertical velocity, heat fluxes, precipitation rate, and moisture convergences are investigated for understanding of the characteristics of the cyclone in more detail. The vector displacement errors in track forecasts are calculated with the estimated best track provided by the India Meteorological Department (IMD). The results indicate that the model is able to capture most of the features of cyclone Mala with reasonable accuracy.

Keywords Tropical cyclone · HWRF model · Track · Intensity · Structure

S. Pattanayak (✉) · U. C. Mohanty
Centre for Atmospheric Sciences, Indian Institute of Technology, Delhi, Hauz Khas,
New Delhi 110016, India
e-mail: sujata05@gmail.com

S. G. Gopalakrishnan
Hurricane Research Division, NOAA, Atlantic Oceanographic and Meteorological Laboratory,
4301 Rickenbacker Causeway, Miami, FL 33149, USA

Published online: 09 June 2011

1 Introduction

Tropical cyclones are organized convective activities, developed over warm tropical oceans. The Indian region is unique in nature than any other region of the world, as far as the genesis/period of occurrence of tropical cyclones and death tolls due to such systems are concerned (Mohanty et al. 2010). The Bay of Bengal is a potentially active region for the development of cyclonic storms, accounting for about 5% of the global annual total number of tropical storms (Mohanty 1994). Though considered to be much weaker in intensity and smaller in size as compared to the cyclones of other regions like Atlantics and Pacific Oceans, the Bay of Bengal cyclones that cross east coast of India and Bangladesh are highly devastating. This is mainly due to shallow bathymetry, nearly funnel shape of the coastline and the long stretch of the low-lying delta region entrenched with a large number of river systems leading to high storm surges and coastal inundations. So the Bay of Bengal tropical cyclone disaster is the costliest and deadliest natural hazard in the Indian sub-continent. Therefore, reasonably accurate prediction of these storms has considerable importance to reduce the significant loss of valuable lives and damage to property.

There have been considerable improvements in the field of weather prediction by numerical models. Recently, a series of high-resolution, non-hydrostatic meso-scale models such as PSU/NCAR Mesoscale Model MM5 (Dudhia 1993), Weather Research Forecasting (WRF) modeling system which includes Advanced Research WRF, i.e., ARW (Skamarock 2005) and Non-hydrostatic Mesoscale Model (NMM), Advanced Regional Prediction System (ARPS) (Xue et al. 2000, 2001), ETA (Black 1994) and Hurricane WRF, i.e., HWRF are used for the simulation/prediction of tropical cyclones. The MM5 has been used in a number of case studies for the simulation of hurricanes over Atlantic (Liu et al. 1997, 1999; Braun et al. 2000; Bao et al. 2000; Zhang and Wang 2003). These simulations have demonstrated the ability of the high-resolution models to reproduce the fine structures in the inner core and outer rain bands in regions of tropical cyclones.

A number of case studies are there for the tropical cyclones over the Bay of Bengal with mesoscale models. Mohanty and Gupta (1997) reviewed in detail the deterministic methods used for tropical cyclone track prediction. Mohanty et al. (2004) used MM5 model to simulate the Orissa super cyclone (1999). Pattanayak and Mohanty (2008) made a comparative study on the performance of both MM5 and WRF models in the simulation of tropical cyclones over Indian seas and demonstrated the superiority of the WRF model over MM5.

The NCEP mesoscale model Hurricane Weather Research and Forecasting (HWRF) system is developed with improved moving nested grid and more complex adaptive grid models (Gopalakrishnan et al. 2002). The skill of the model is demonstrated through prediction of difficult track scenarios that include erratically moving storms, storms that accelerate and storms that stall. The convective systems like tropical cyclones are mainly influenced by the large-scale phenomenon. Hence, high-resolution models are desirable to capture the complexity in the surface wind as well as better track representation. Due to the computer constraints, it is difficult to integrate the whole domain of interest with a very high resolution. The HWRF model prevails over all such constriction and designed in such a way that the outer large domain will capture all the large-scale information and with that the high-resolution inner nest will move as the storm moves. In this way, large-scale information is not discarded and at the same time, the complex structure of the storm can be captured. This is the main purpose of using the HWRF model, and thus, it is expected to

be a suitable modeling system for prediction of tropical cyclones in the Indian seas. Therefore, in the present study, in order to evaluate performance of the NCEP/NOAA mesoscale HWRF modeling system (atmospheric component), a very severe cyclonic tropical cyclone Mala developed over Bay of Bengal is simulated with six different initial conditions.

A description of the mesoscale model HWRF used in the present study is given in Sect. 2. The synoptic situation of the cyclone Mala is provided in Sect. 3. The numerical experiments carried out along with data used for the present study are explained in Sect. 4. Model simulated results are given in Sect. 5 in order to evaluate the performance of the model over Indian seas with the conclusions in Sect. 6.

2 Model description

The Weather Research and Forecast system for hurricane prediction i.e. HWRF system was developed by the Environmental Modeling Center (EMC)/National Centers for Environmental Prediction (NCEP). In the present study, the atmospheric component of the HWRF system is used. It is designed to be a flexible, state-of-the-art atmospheric simulation system that is efficient on available single as well as parallel computing platforms. The HWRF model is a fully compressible, non-hydrostatic model with a hydrostatic option (Janjic et al. 2001; Janjic 2003). The model uses the rotated lat-long projection that minimizes the convergence over meridians over the domain and the Arakawa E-grid staggering for computational efficiency. The terrain following hybrid sigma-pressure vertical coordinate system is used. The dynamics conserve a number of first- and second-order quantities including energy and enstrophy (Janjic 1984). Forward–backward schemes are used for the horizontally propagating fast-waves, and implicit scheme is used for the vertically propagating sound waves. Adams–Bashforth scheme and Crank–Nicholson scheme are used for horizontally and vertically propagating waves. The basic model equations and the brief descriptions on the discretization of model equations are provided in Appendix 1. The Geophysical Fluid Dynamics Laboratory (GFDL) long-wave and short-wave radiation schemes are incorporated in the model. The GFDL long-wave radiation scheme has the multi-band, transmission table look-up scheme with carbon dioxide; ozone and water vapor absorptions (Fels and Schwarzkopf 1975; Schwarzkopf and Fels 1985; Schwarzkopf and Fels 1991) in which cloud microphysics effects are included. The GFDL short-wave radiation scheme has two spectral bands, k-distribution scheme with ozone and water vapor as the main absorbing gases (Lacis and Hansen 1974) and cloud microphysics effects are also included. It has a well-tested NCEP GFS scheme for planetary boundary layer parameterization (Hong and Pan 1996). The PBL height is determined using an iterative bulk-Richardson approach working from the ground upward, whereupon the profile of the diffusivity coefficient is specified as a cubic function for the PBL height. The diffusivity coefficient values are obtained by matching the surface layer fluxes. A counter-gradient flux parameterization is included. The Simplified Arakawa-Schubert cumulus parameterization scheme is used (Arakawa and Schubert 1974; Grell 1993). The moving structure of inner nest along with the automatic tracking system of tropical cyclones and diagnosis of its intensity and structure enhances the importance of the HWRF modeling system. Table 1 summarizes the model configuration and various options of the HWRF model used for the numerical experiments.

Table 1 HWRF model description

Model	Hurricane WRF of NCEP/NOAA, Version 2.1
Dynamics	Non-hydrostatic with terrain following hybrid pressure sigma vertical co-ordinate
Map projection	Mercator
Horizontal grid distance	27 km (Domain-1), 9 km (Domain-2)
Number of vertical level	43 sigma levels
Horizontal grid scheme	Arakawa E-grid
Time integration scheme	Horizontally: forward–backward scheme
	Vertical: implicit scheme
Initial & lateral boundary condition	GFS analysis & forecast
Radiation scheme	Long wave: GFDL scheme
	Short wave: GFDL scheme
Planetary boundary layer parameterization scheme	NCEP global forecast system scheme
Land surface	NMM Land surface scheme
Cumulus parameterization scheme	Simplified Arakawa Schubert scheme
Microphysics	Ferrier scheme
Topography	30 s elevation data (USGS)
SST & surface parameters	GFS analysis & forecast

3 System description

The cyclone Mala was genesis near 9.5°N, 90.5°E, over the Bay of Bengal at about 03 UTC 25 April 2006 as a well-marked low-pressure with the minimum central sea level pressure (CSLP) of 996 hPa and the maximum surface wind (MSW) of 13 m/s. The system remained in that stage for further 6 h, i.e., up to 09 UTC 25 April 2006. By 09 UTC 25 April 2006, the system intensified to a deep depression stage. The system became cyclonic storm after 12 UTC 25 April 2006. At 00 UTC 26 April 2006, well-developed cyclonic storm with the center of the storm at 10.5°N and 89.0°E with CSLP of 994 hPa and MSW of 23 m/s was observed. The system remained in cyclonic stage up to 00 UTC 27 April 2006 and around 03 UTC 27 April 2006; it further intensified to a severe cyclonic storm with CSLP of 990 hPa and the MSW of 28 m/s. The system became very severe cyclonic storm (VSCS) by 12 UTC 27 April 2006 with CSLP of 984 hPa and the MSW of 34 m/s. The storm remained in VSCS for a period of 42 h, i.e., up to 06 UTC 29 April 2006. The deepening of the central pressure was 954 hPa with the pressure drop of 52 hPa, and the observed MSW was 51 m/s. The storm crossed the Arakan coast (17.5°N, 94.5°E) at about 100 km south to Sandoway around 07 UTC 29 April 2006. The system remained on the land for further 12 h and caused a lot of devastation in the underlying coastal areas. The observed best-fit track as well as the CSLP in every 06-h interval is illustrated in Fig. 1.

Environmental condition was also favorable for strengthening the tropical cyclone Mala to almost super cyclone stage before landfall. The wind shear (10–20 mps) between mid & upper levels initially inhibited the intensification of the system irrespective of the sea surface temperature (SST) values of the order of 28–29°C over the area. Later on when the rapid intensification into a VSCS occurred during 27 & 28, the wind shear had become quite negligible (i.e. of the order of 5–10 m/s). Also, the system followed the

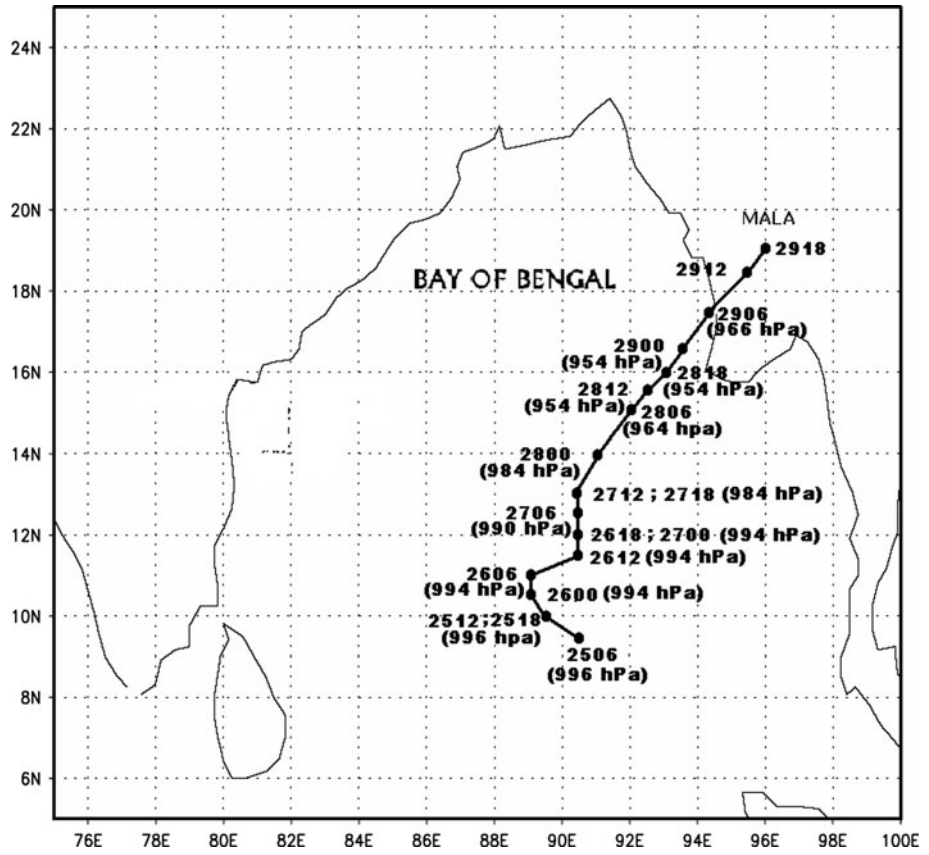

Fig. 1 Best-fit tracks of severe tropical cyclone Mala (26–29 April 2006) over the Bay of Bengal during the year 2006 (Majumdar et al. 2007)

climatological track. Out of the total 31 systems formed during the period of April since 1877 till 2005, in the Bay of Bengal, 27 had moved toward Arakan coast, 1 toward Bangladesh (Chittagong), and 3 toward Tamil Nadu coast (IMD 2007).

4 Numerical experiments and data used

The HWRF model described in Sect. 2 is integrated up to 96 h in a nested domain configuration. The geographical domain used in the present study is illustrated in Fig. 2. The outer domain of 27 km (fixed domain) and the inner domain of 9 km (moving nest) are used for model integration. The model has 43 levels up to a height of 30 km in the vertical and the model is integrated with time step of 60 s for the outer domain and 20 s for inner nest. A single case or single initial condition cannot provide performance evaluation of any model. Hence, the performance of the model is evaluated with different initial condition. For this purpose, the model is integrated with six different initial conditions, i.e., 00 UTC 25 April 2006, 12 UTC 25 April 2006, 00 UTC 26 April 2006, 12 UTC 26 April 2006, 00 UTC 27 April 2006, and 12 UTC 27 April 2006. The initial and lateral boundary conditions to a limited area model are usually provided from the large-scale analysis of different NWP

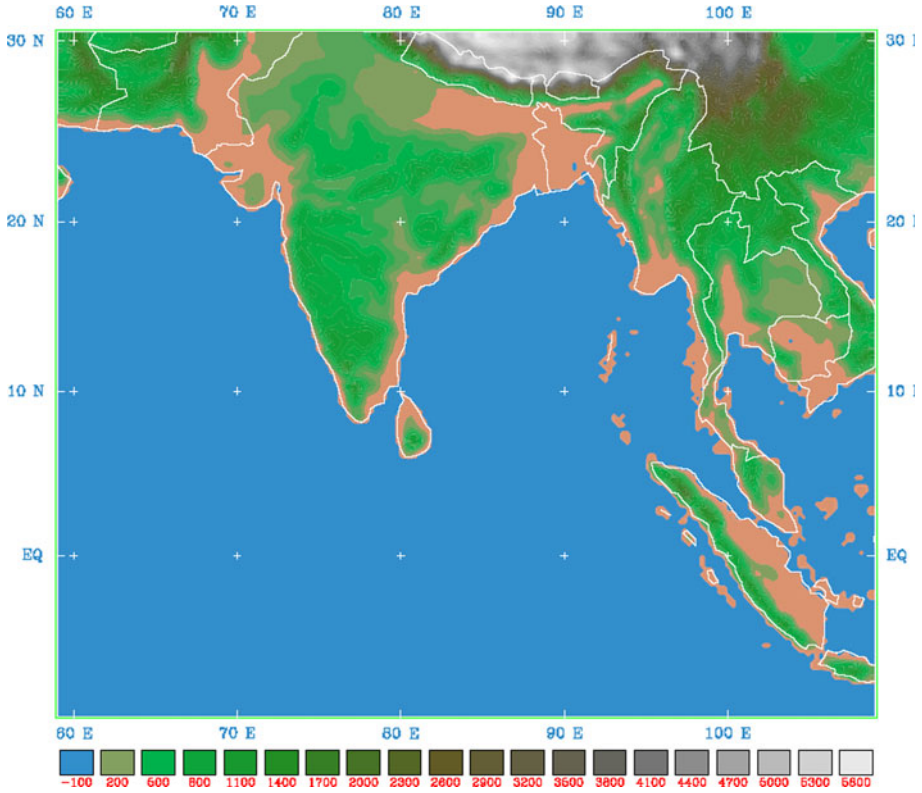

Fig. 2 Model geographical domain used for the present study

centers in the world. The NCEP Global Forecast System (GFS) analysis and forecasts ($1° \times 1°$ horizontal resolution) have been used to provide the initial and lateral boundary conditions, respectively.

5 Results and discussions

The results as obtained from the model simulations are presented in this section. Model simulated CSLP, wind at 850 and 200 hPa, precipitation and tracks of the cyclone with a few diagnostic fields such as heat fluxes, convective heating zone, relative vorticity, pressure vertical velocity, and moisture convergence are described in this section. The time series plots of minimum central pressures and maximum sustainable surface winds for different initial conditions are also calculated. The vector displacement errors in tracks forecasts and error in CSLP and MSW for intensity forecasts with different initial conditions are also evaluated.

5.1 Tracks of the cyclone Mala

The model is integrated for 96 h with different initial conditions as stated earlier. Figure 3 represents the tracks of the cyclone Mala from model simulations with six initial conditions

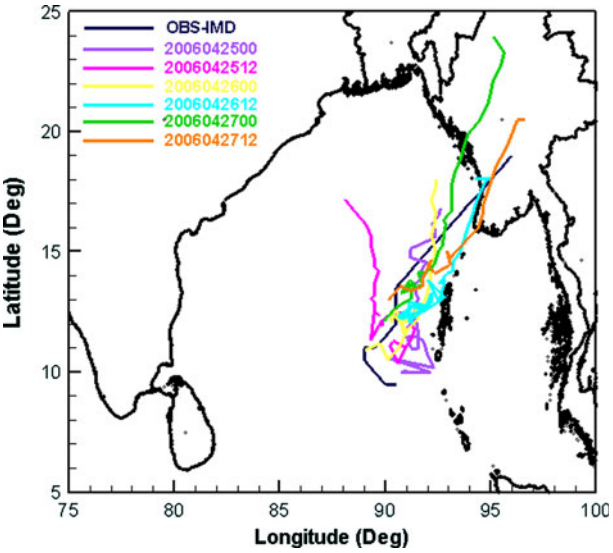

Fig. 3 Tracks of the cyclone Mala with different initial conditions

and also provided the observed initial location as estimated by India Meteorological Department (IMD). From Fig. 3, it is clearly seen that all the tracks except the track from the initial condition of 12 UTC 25 April 2006 are moving towards the Arakan coast and almost along the observed track. Also, the tracks from the initial condition of 00 UTC 25 April 2006, 12 UTC 25 April 2006, and 00 UTC 26 April 2006 do not show any landfall of the cyclone up to 96 h of simulation time. This is due to slow movement of the simulated cyclone during these initial conditions. All the other initial conditions, i.e., 12 UTC 26 April 2006, 00 UTC 27 April 2006, and 12 UTC 27 April 2006 are well predicted, the track of Mala with reasonable accuracy. The vector displacement errors (VDE) are also calculated with IMD estimated location of the storm at every 12 h interval for each simulated track, which is presented in Fig. 4. From the figure, it is clearly seen that at the initial time of model integration, large positional error of the cyclone in the range of 40–195 km is estimated from different initial conditions.

5.2 Intensity prediction

Figure 5a, b represents the intensity prediction of cyclonic storm Mala in terms of minimum CSLP in hPa and MSW in m/s, respectively. The observed minimum CSLP as estimated by IMD was 954 hPa, whereas the results from the initial conditions of 00 & 12 UTC 25 and 00 UTC 26 April 2006 show much higher intensity than the observed value. The model simulation from the initial condition of 00 UTC 27 April 2006 provides more accurate result in terms of minimum CSLP (hPa) and MSW (m/s) than all other initial conditions. Also, the errors in minimum CSLP (hPa) and MSW (m/s) are evaluated and presented in Fig. 6a, b, respectively. The error in intensity prediction is calculated as the difference between simulated value at different initial conditions and the corresponding estimated value from IMD. This has been used for both CSLP and MSW error calculation. The errors in CSLP simulation clearly shows that the initial condition of 00 UTC 27 April 2006 produces comparatively less error than other initial conditions up to 96 h except at

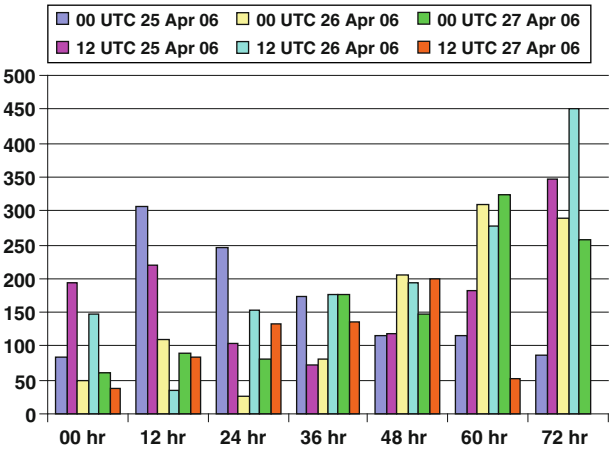

Fig. 4 Vector displacement errors (km) for cyclone Mala with different initial conditions

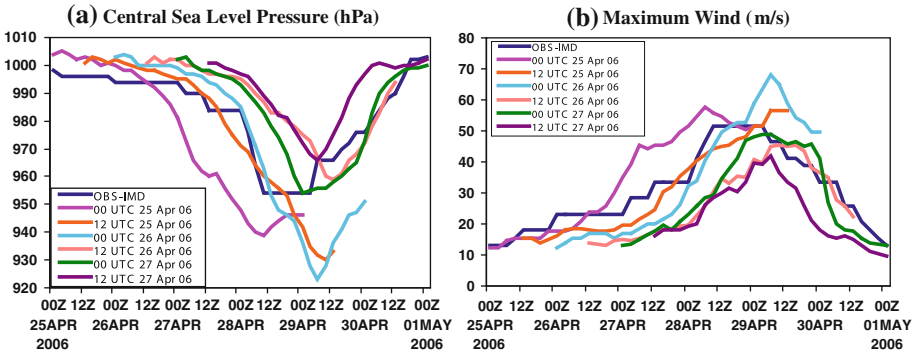

Fig. 5 **a** Central sea level pressure (*CSLP*) (hPa) and **b** maximum sustainable surface wind (m/s) for cyclone Mala with different initial conditions

36 h of simulation. Similarly, the MSW is well simulated with the initial condition of 00 UTC 27 April 2010. Hence, the large-scale fields as well as the structure of the cyclone are further investigated from the results as obtained with the initial condition of 00 UTC 27 April 2010.

5.2.1 Central sea level pressure

Figure 7 represents the CSLP from both domain-1 and domain-2 valid with the area coverage as of inner domain. Figure 7a represents the initial analysis (initial condition) for the model integration valid at 00 UTC 27 April 2006. In the initial analysis, the CSLP is 1,002 hPa and IMD reported the CSLP of 994 hPa. Figure 7b–d represents verifying analysis, day-1 forecast for domain-1 and day-1 forecast for domain-2, respectively, valid at 00 UTC 28 April 2006. In the verifying analysis, the CSLP is 999 hPa, whereas in the forecast, the CSLP is 993 hPa for domain-1 and 989.5 hPa for domain-2, respectively. The observed CSLP for the corresponding time is 984 hPa. So, from a very low intensity in the

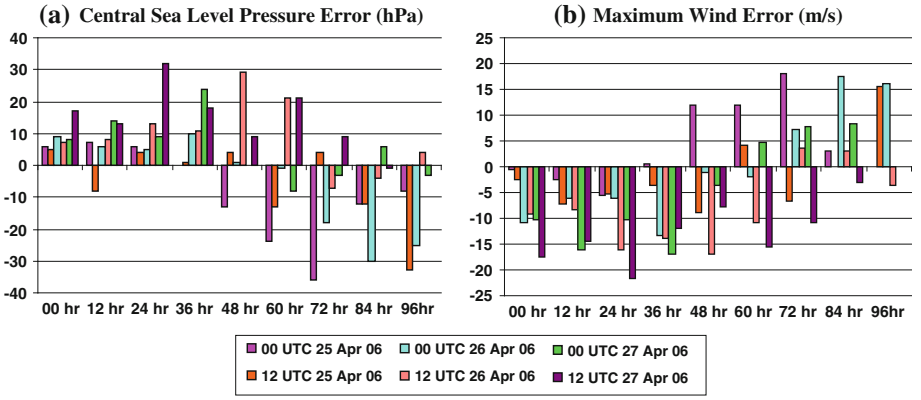

Fig. 6 Intensity errors for **a** MSLP (hPa) and **b** maximum sustainable surface wind (m/s)

large-scale analysis, model is able to simulate an intensified storm by 24-h forecast. Also, domain-2 simulates the CSLP reasonably well than domain-1. Figure 7e–g represents the verifying analysis, day-2 forecast for domain-1 and day-2 forecast for domain-2, respectively valid at 00 UTC 29 April 2006. In verifying analysis, the CSLP is 997.5 hPa and the system is very nearer to the land, whereas the model simulation shows the peak intense stage of the storm by this time and could simulate the central CSLP of 952 hPa in the high-resolution nested domain. The estimated CSLP at that time was 954 hPa. So, instead of a very low intensity and coarse resolution in the initial and boundary condition from GFS analysis and forecast, the model is able to predict the storm intensity reasonably well. The maximum observed pressure drop was 52 hPa, whereas the outer mother domain could simulate the pressure drop of 41 hPa and the inner nested domain could simulate the pressure drop of 55 hPa (not shown). However, the simulated CSLP at the nested domain exhibit higher values than observed central pressure. Model simulated results (all the figures not shown) clearly demonstrate the intensification and dissipation of the storm realistically. The details of the central sea level pressure and pressure drop with the initial condition of 00 UTC 27 April 2006 are presented in Table 2.

5.2.2 Wind at 850 hPa and 200 hPa

Figure 8 represents the wind at 850 hPa from both domain-1 and domain-2 with area coverage as of inner domain. Figure 8a represents verifying analysis at the initial time of the model integration. Figure 8b–d represents the verifying analysis, day-1 forecast for domain-1 and day-1 forecast for domain-2 from the model simulation, respectively, valid at 00 UTC 28 April 2006. In the analysis, the system is found to be stronger in the southern sector and slightly elongated in north south direction. In the forecast, wind is stronger in the south east sector and the simulated wind field is more circular around the storm. Figure 8e–g represents the verification analysis, day-2 forecast for domain-1 and the day-2 forecast for domain-2, respectively, valid at 00 UTC 29 April 2006. The maximum intensity of 68 m/s is simulated by the model in the nested domain. Model simulated result (all the figures not shown) clearly demonstrates the intensification and dissipation of the storm.

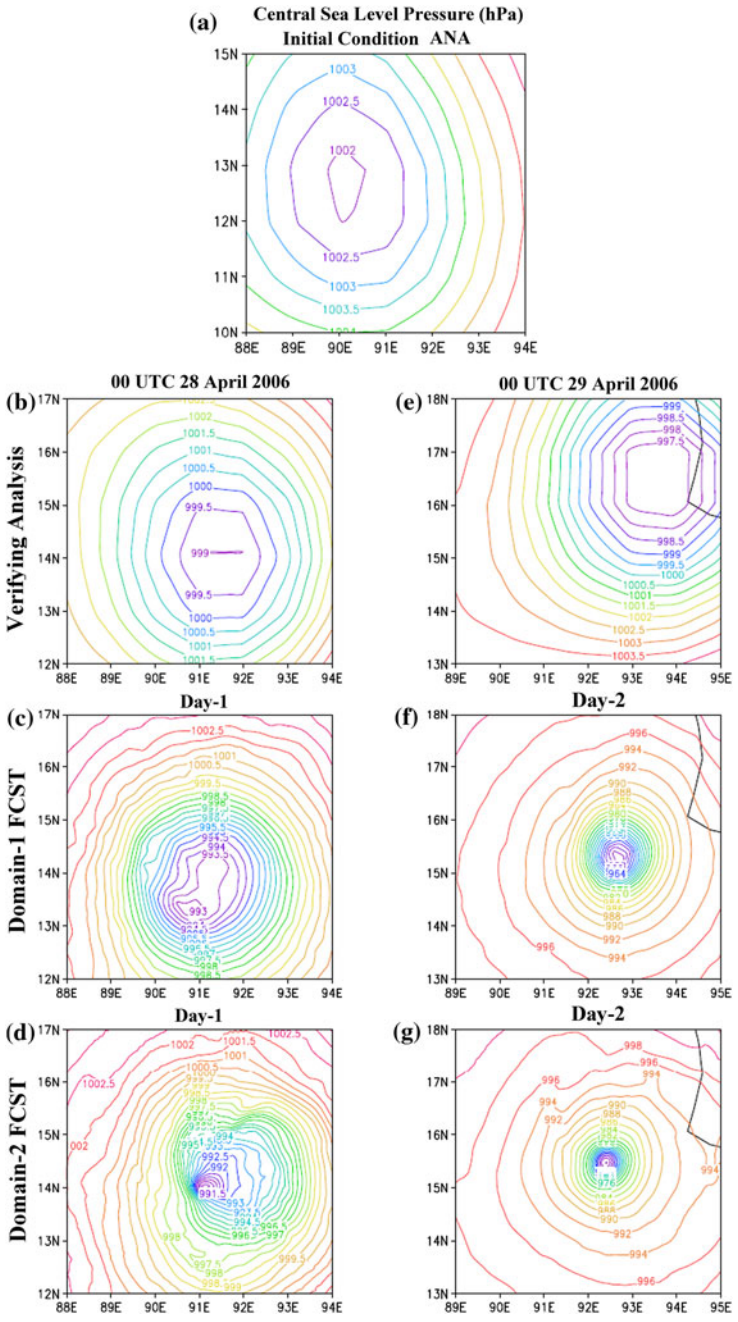

Fig. 7 Central sea level pressure. **a** Initial condition (*ANA*) valid at 00 UTC 27 April 2006, **b** verifying analysis, **c** domain-1 forecast, and **d** domain-2 forecast valid at 00 UTC 28 April 2006. **e**–**g** are same as **b**–**d** but valid at 00 UTC 29 April 2006

Table 2 Observed & model simulated central sea level pressure and pressure drop (hPa) for the Bay of Bengal cyclone Mala

Date and time	Observed		Simulated			
	Central pressure (hPa)	Pressure droop (hPa)	Central pressure (hPa)		Pressure droop (hPa)	
			Domain-1	Domain-2	Domain-1	Domain-2
00 UTC 27 April 2006	994	6	1,002	1,001	2	3
12 UTC 27 April 2006	984	10	997	996	5	6
00 UTC 28 April 2006	984	22	993	989	9	12
12 UTC 28 April 2006	954	52	978	972	19	25
00 UTC 29 April 2006	954	52	954	952	28	30
12 UTC 29 April 2006	966	50	958	956	41	43
00 UTC 30 April 2006	980	26	973	972	30	31
12 UTC 30 April 2006	1,002	3	996	992	3	5
00 UTC 01 May 2006	1,003	2	1,000	1,000	3	3

Figure 9 demonstrates the wind at 200 hPa for both the domains with area coverage as of nested domain. Figure 9a represents the verifying analysis at the initial time of the model integration valid at 00 UTC 27 April 2006. Figure 9b–d represents the verifying analysis, day-1 forecast for domain-1 and day-1 forecast for domain-2 from the model simulation, respectively, valid at 00 UTC 28 April 2006. In the analysis, the upper level divergence is clearly noticed. Day-1 forecast clearly shows the upper level divergence in both the domains and the magnitude is well predicted. Figure 9e–g represents the verification analysis, day-2 forecast for domain-1 and the day-2 forecast for domain-2, respectively, valid at 00 UTC 29 April 2006. The wind patterns as well as the divergence are well simulated by the model.

Model-simulated 10-m wind is also compared with that of the observation (figures not shown). In 24 h (day-1), model could simulate the 10-m wind speed as 23 and 31 m/s in the outer and inner domain, respectively, whereas the observed wind speed is 35 m/s at that time. In 48 h, the outer domain could simulate 10-m wind as 42 m/s and the inner domain could simulate the 10-m as 47 m/s, whereas the observed wind speed is 51 m/s. Hence, the wind distribution in terms of magnitude and pattern and 10-m wind is well simulated by the model. Also, the high-resolution nested domain could simulate the storm intensity much closer to that of estimated value. Again, in spite of very low intensity in the initial condition, the model is able to predict the storm intensity reasonably well.

5.2.3 Precipitation

Figure 10 represents 24-h accumulated precipitation from Tropical Rainfall Measuring Mission (TRMM) and model simulation. The TRMM precipitation (3B42) data sets are the merged analysis of Tropical Rainfall Measuring Mission (TRMM), TMI and rain gauges observations carried out by National Aeronautics and Space Administration (NASA) and obtained from the NASA Web site (http://disc2.nascom.nasa.gov/Giovanni/tovas). Figure 10a, b represents 24-h accumulated precipitation as estimated from TRMM and model simulation, respectively, valid at 03 UTC 28 April 2006. The TRMM estimated precipitation was about 17 cm, whereas model could simulate the precipitation of 14 cm valid at the same time. Figure 10c, d represents 24-h accumulated TRMM precipitation and day-2

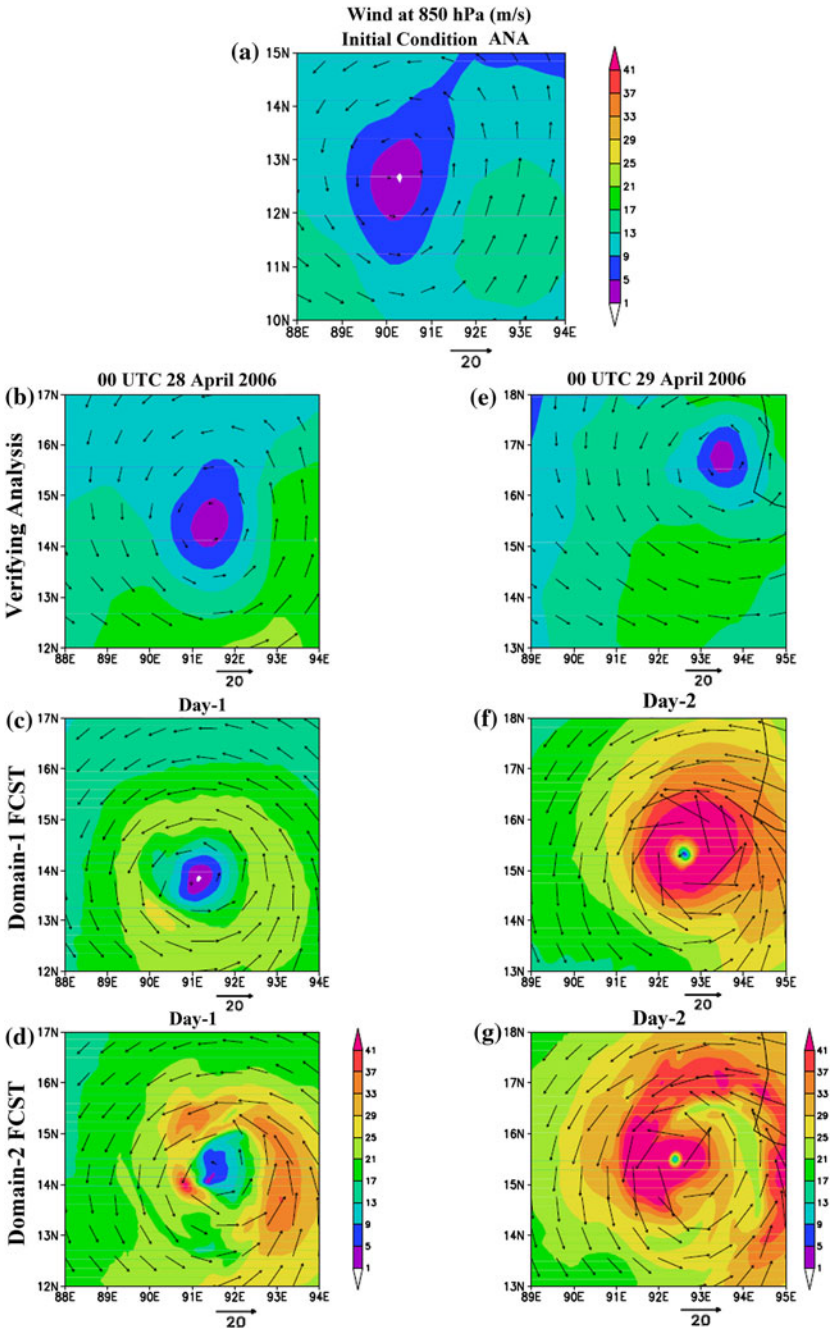

Fig. 8 Wind at 850 hPa. **a** Initial condition (*ANA*) valid at 00 UTC 27 April 2006, **b** verifying analysis, **c** domain-1 forecast, and **d** domain-2 forecast valid at 00 UTC 28 April 2006. **e**–**g** are same as **b**–**d** but valid at 00 UTC 29 April 2006

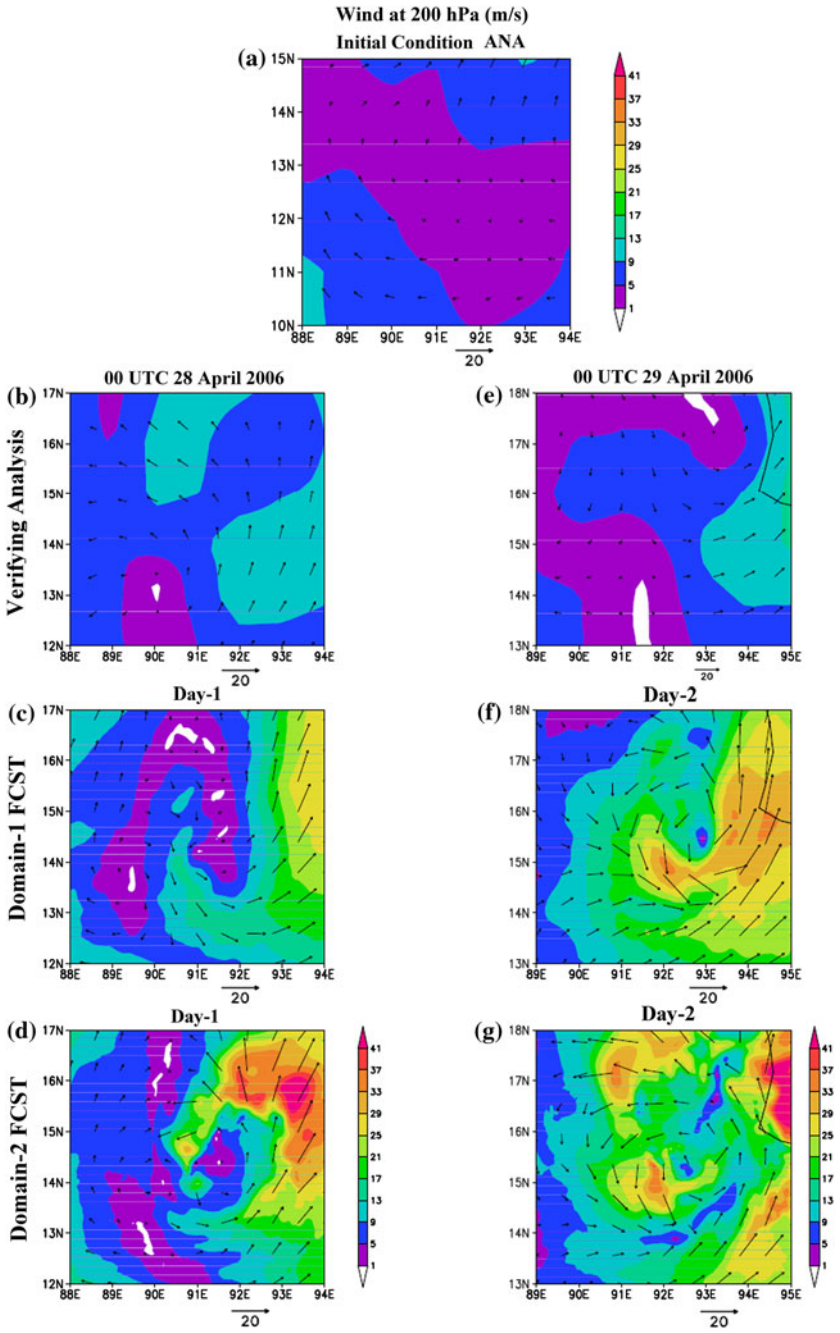

Fig. 9 Wind at 200 hPa. **a** Initial condition (*ANA*) valid at 00 UTC 27 April 2006, **b** verifying analysis, **c** domain-1 forecast, and **d** domain-2 forecast valid at 00 UTC 28 April 2006. **e**–**g** are same as **b**–**d** but valid at 00 UTC 29 April 2006

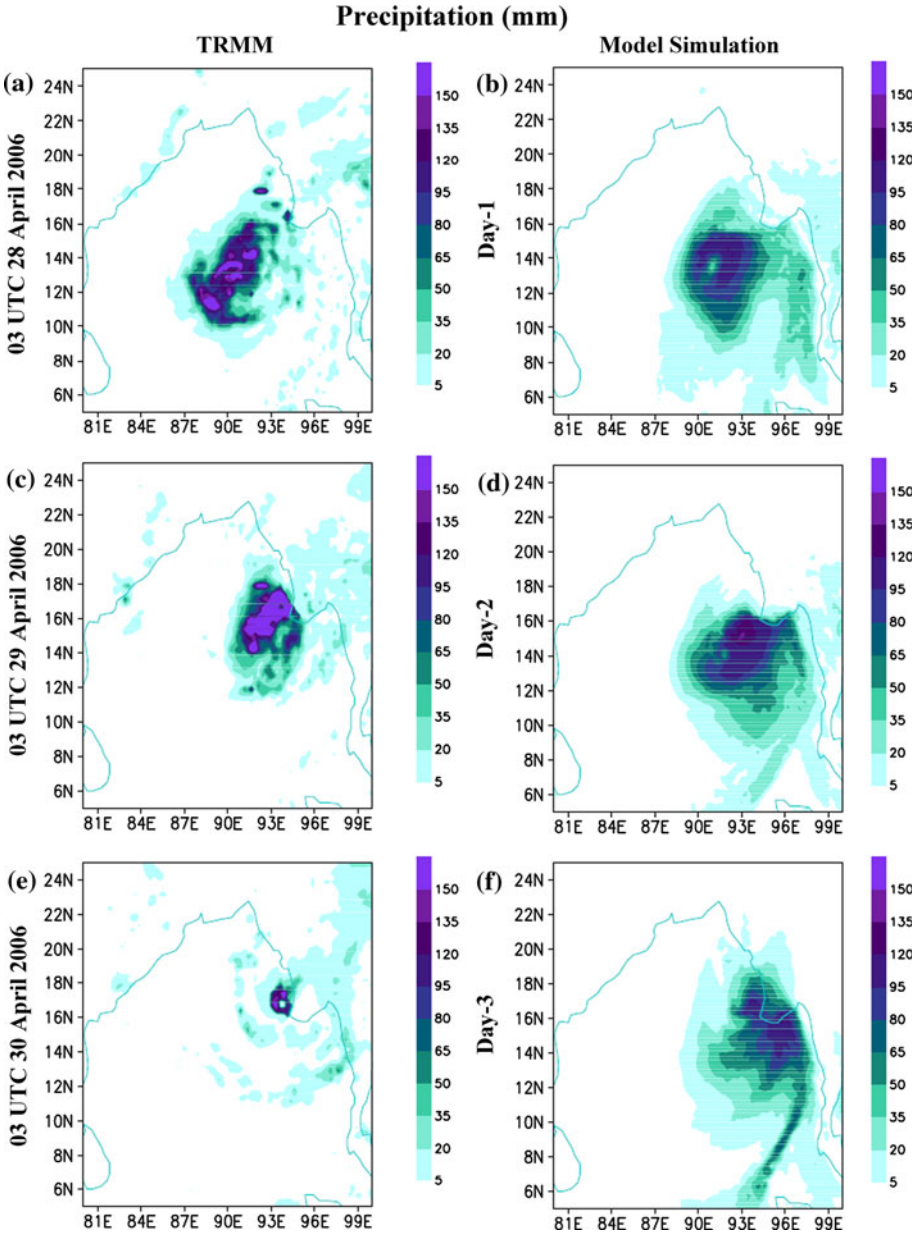

Fig. 10 Twenty-four hour accumulated precipitation (mm). *Left panel* is from TRMM precipitation valid at **a** 03 UTC 28 April 2006, **c** 03 UTC 29 April 2006, and **e** 03 UTC 30 April 2006 and *right panel* is corresponding model simulations

forecast from model simulation valid at 00 UTC 29 April 2006. The TRMM estimated precipitation was about 18 cm, whereas the model could simulate the precipitation of 13 cm valid at the same time. Figure 10e, f represents 24-h accumulated TRMM precipitation and day-3 forecast from model simulation valid at 00 UTC 30 April 2006. The

TRMM estimated precipitation was about 16 cm, where as the model could simulate the precipitation of 23 cm.

Thus, it may be noted that the model underestimates precipitation amount in day-1 and day-2 forecast and overestimates precipitation on day-3. Also, day-3 forecast clearly shows very wide spread of precipitation than the observed precipitation. In respect of the pattern of distribution of the precipitation around the center of the cyclone, model could simulate reasonably well. It is consistent with the intensity of the tropical cyclone simulation.

5.3 Structure of the cyclone Mala

It has been attempted to study the inner core structure of Mala with model simulation. The intensity prediction has been further investigated through the Hovmoller diagrams of latent heat flux, sensible heat flux, convective, and large-scale precipitation. The latent heat flux is one of the dominant components of the air-sea energy exchange process associated with tropical cyclones. The higher the intensification of the storm, the higher should be the flux values (Mandal et al. 2007). Figure 11a represents the time series of the maximum values of the latent heat flux (LHF) in the radius of influence of the storm. It clearly shows that the maximum LHF of 1,105 Wm^{-2} is simulated at 06 UTC 29 April 2006. Figure 11b represents the time series of the maximum values of the sensible heat flux (SHF) in the radius of influence of the storm for both the domains. It clearly shows the maximum value of 300 Wm^{-2} is simulated by the model valid at 03 UTC 29 April 2006. Also, Wong and Yip (2005a, b) investigate the motion of the tropical cyclone in response to the heat flux values using the MM5 model and concluded that the heat flux can affect the motion of the tropical cyclone as well as to the high vertical velocity of the storm. Thus, it may be noted that model could simulate the heat fluxes in terms of latent heat flux and sensible heat flux reasonably well (Mandal et al. 2007).

Also, the characteristics of simulated precipitation further examined from distribution of convective and large-scale precipitations and corresponding heating zones. Figure 11c, d represents the 3-h time series of convective and large-scale precipitation (mm). The maximum convective precipitation of 16 cm and large-scale precipitation of 55 cm are simulated. The possible cause for the sharp increase in the large-scale precipitation is further investigated by analyzing the deep convective heating (°K/day) and large-scale condensation heating (°K/day) zones which are provided in Fig. 11e and f, respectively. The deep convective heating is found in between 500 and 300 hPa and as the convection is going on at each stages of tropical cyclone, the precipitation due to convection is well captured by the model which is represented in Fig. 11c. However, the large-scale precipitation has a sudden rise with the maximum value of 55 cm at intense period of the cyclone. This could be attributed to large-scale condensation heating, which is comparatively more during the intense period of the cyclone and is well extended from 800 to 300 hPa with the maximum value of 25°K/day.

Furthermore, the structure of the cyclone is demonstrated through the vertical structure of relative vorticity ($\times 10^{-5}$ s^{-1}), moisture flux, east–west cross section of horizontal wind (m/s) and pressure vertical velocity (m/s). Figure 12a represents the Hovmoller diagram of relative vorticity ($\times 10^{-5}$ s^{-1}). The positive vorticity is extended up to 400 hPa with the negative vorticity at the upper levels. The maximum positive relative vorticity of 75×10^{-5} s^{-1} is simulated at 800 hPa and in the time window of 00 UTC to 12 UTC 29 April 2006. This matches with the observed maximum intensity time of the cyclone. Figure 12b represents the Hovmoller diagram of vertically integrated moisture flux. The results clearly indicate low level convergence and upper level divergence. The maximum

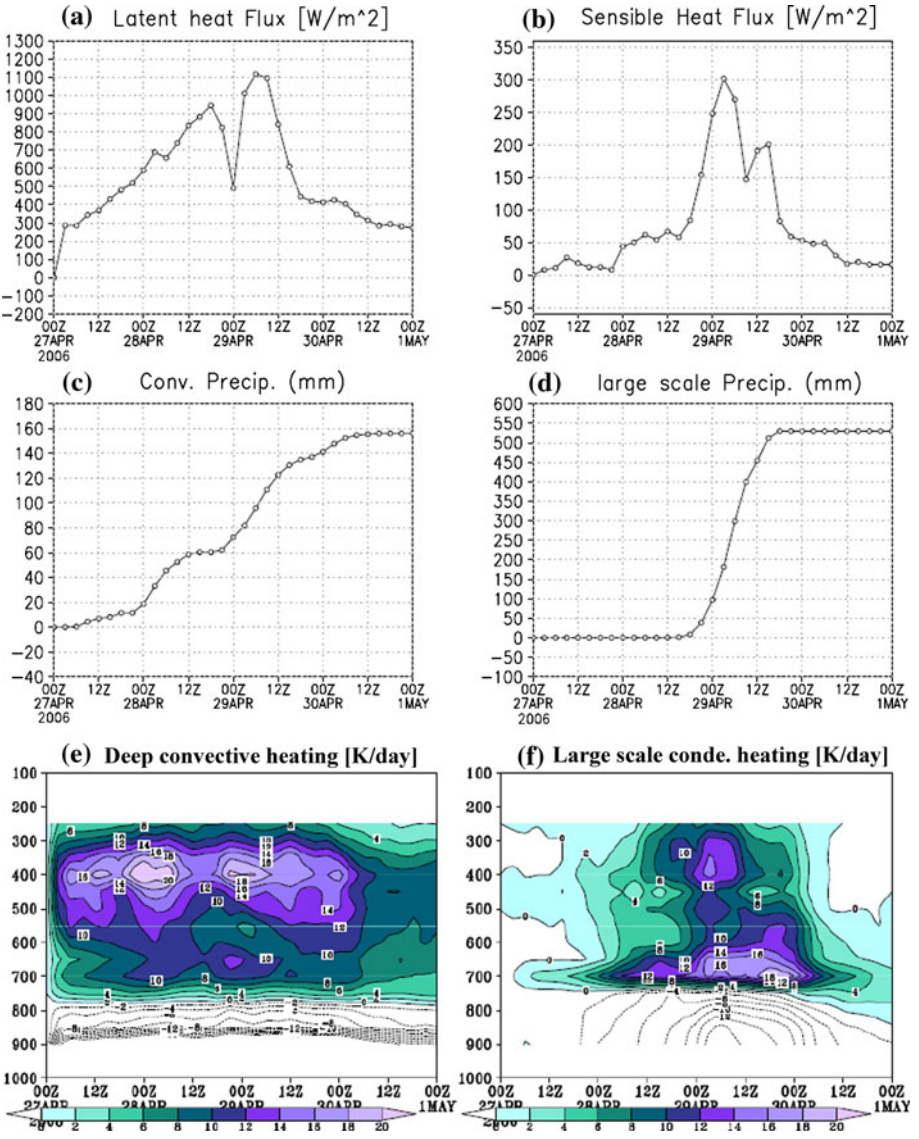

Fig. 11 Time series of **a** latent heat flux (Wm^{-2}), **b** sensible heat flux (Wm^{-2}), **c** convective precipitation (mm), **d** large-scale precipitation (mm), **e** deep convective heating (K/day), and **f** large-scale condensation heating (K/day)

convergence is simulated at 00 UTC 29 April 2006, which is 9 h prior than the landfall time. The moisture flux of the order of −80 to 95 is simulated with the initial condition of 00 UTC 27 April 2006. Figure 12c demonstrates the east–west cross section of horizontal wind speed crossing through the center of the cyclone. The horizontal wind is minimum at the center of the storm and maximum at both sides of the center of the storm. However, right side of the center of the storm exhibits maximum wind (50 m/s) between 700 and 400 hPa, and in the left side, the horizontal wind exhibits maximum (45 m/s) near the surface. Figure 12d represents the pressure vertical velocity that shows the heating dipole

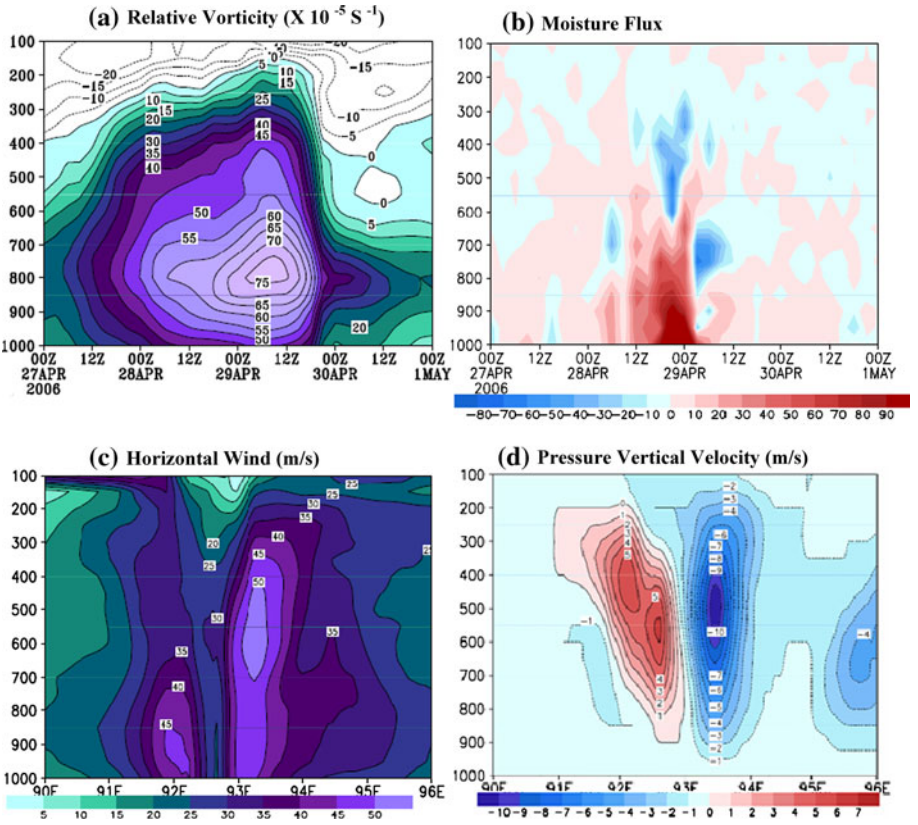

Fig. 12 Hovmoller diagram of **a** relative vorticity ($\times 10^{-5}$ s−1), **b** moisture flux, **c** east–west cross section of horizontal wind (m/s), and **d** pressure vertical velocity (m/s)

liable for the potential vorticity generation which is isolated within the band. Also, the updraft and downdraft increases the intensity of the storm. The strong updraft of 6 m/s and downdraft of 10 m/s are evaluated from the model simulation. However, the strong updraft is seen at 600 hPa.

6 Conclusion

The present study on the performance of the state-of-the-art non-hydrostatic hurricane forecasting model in simulation of Bay of Bengal tropical cyclone leads to the following conclusions.

The model could simulate most of the features of cyclone Mala over the Bay of Bengal with reasonable accuracy. The tracks forecasts from different initial conditions clearly show that each track except the track from the initial condition of 12 UTC 25 April 2006 moves toward Arakan coast with a spread of about 200 km.

The intensity forecast in terms of Central Sea Level Pressure (CSLP) and Maximum Sustainable Wind is well captured by the model, with an over estimation in some of the initial conditions. Moreover, the high-resolution inner nest produces higher intensity of the storm than the outer domain. At the same time, with a very low intensified analysis field

(GFS), the model is able to simulate the severe cyclonic storm with the CSLP of 954 hPa with the initial condition of 00 UTC 27 April 2006.

The amount and spatial distribution of precipitation are well simulated by the model. Model simulation underestimates the precipitation amount on day-1 (03 UTC 28 April 2006) and day-2 (03 UTC 29 April 2006) forecast, whereas it overestimates on day-3 valid at 03 UTC 30 April 2006. Also, the convection and large-scale precipitation clearly demonstrate that the convection and condensation heating zones are well matched with the simulation of precipitation.

The simulation of various meteorological fields in the inner core of the cyclone Mala clearly illustrates broad characteristics of the structure of the severe tropical cyclone. Further, the Hovmoller diagram of relative vorticity clearly demonstrates the positive vorticity of 75×10^{-5} s^{-1} in the lower level and negative vorticity of 20×10^{-5} s^{-1} in the upper level. The strong horizontal wind, vertical velocity, and moisture flux clearly represent the severity of the cyclone Mala.

Acknowledgments The Indian National Center for Ocean Information Services (INCOIS), Ministry of Earth Sciences (MoES) is gratefully acknowledged for providing financial support to carry out this research. The authors acknowledge the Environmental Modeling Center (EMC) of NCEP for providing HWRF modeling system for the present study. The authors owe thanks to India Meteorological Department (IMD) for providing best track parameters of the storm and NASA for precipitation data sets for the validation of the model simulated results. The authors gratefully acknowledge the NCEP/NCAR for their analysis and forecast data sets used in the study.

Appendix 1

HWRF modeling system

HWRF is a fully compressible Eulerian non-hydrostatic coordinate system with a hydrostatic option. The horizontal rotated latitude-longitude coordinate and the vertical terrain following hydrostatic-pressure-based sigma coordinate system is used. The sigma coordinate system is up to a specified pressure surface usually below the tropopause, and hydrostatic pressure coordinate above. Top of the model is a constant pressure surface.

Model formulation

The vertical sigma coordinate is defined as,

$$\sigma = \frac{\pi - \pi_t}{\mu}$$

$$\mu = \pi_s - \pi_t$$

where π is the hydrostatic pressure, π_s stands for the hydrostatic pressure at the surface, π_t represents the hydrostatic pressure at the top of the model atmosphere.

Then the equations governing a dry, inviscid and adiabatic non-hydrostatic atmosphere are (Janjic et al. 2001),

$$\frac{\partial \mathbf{v}}{\partial t} = -\mathbf{v} \cdot \nabla_\sigma \mathbf{v} - \dot{\sigma} \frac{\partial \mathbf{v}}{\partial \sigma} - (1+\varepsilon)\nabla_\sigma \Phi - \alpha \nabla_\sigma p + f\mathbf{k} \times \mathbf{v} \qquad \text{(Horizontal momentum)}$$

$$\frac{\partial T}{\partial t} = -\mathbf{v} \cdot \nabla_\sigma T - \dot{\sigma} \frac{\partial T}{\partial \sigma} + \frac{\alpha}{C_p}\left[\frac{\partial p}{\partial t} + \mathbf{v} \cdot \nabla_\sigma p + \dot{\sigma} \frac{\partial p}{\partial \sigma}\right] \qquad \text{(Thermodynamic)}$$

$$\frac{\partial \mu}{\partial t} + \nabla_\sigma \cdot (\mu \mathbf{v}) + \frac{\partial (\mu \dot{\sigma})}{\partial \sigma} = 0 \qquad \text{(Continuity)}$$

$$\frac{\partial p}{\partial \pi} = 1 + \varepsilon \qquad \text{(Vertical equation of motion)}$$

$$\frac{\partial \Phi}{\partial \sigma} = -\mu \frac{RT}{p} \qquad \text{(Hypsometric)}$$

$$w = \frac{1}{g}\frac{\mathrm{d}\Phi}{\mathrm{d}t} = \frac{1}{g}\left(\frac{\partial \Phi}{\partial t} + \mathbf{v} \cdot \nabla_\sigma \Phi + \dot{\sigma}\frac{\partial \Phi}{\partial \sigma}\right) \qquad \text{(Non-hydrostatic continuity)}$$

$$\alpha = {}^{RT}/_{p} \qquad \text{(Equation of state)}$$

$$\varepsilon = \frac{1}{g}\frac{\mathrm{d}w}{\mathrm{d}t} \qquad \text{(Definition of } \varepsilon\text{)}$$

where $\mathbf{v}$ is the horizontal wind vector, p is the non-hydrostatic pressure, R is the gas constant for dry air, T is temperature and Φ is geopotential.

It is to be noted that, Φ, w, and ε are not independent and there is no independent prognostic equations for w. Instead, w is computed diagnostically from the non-hydrostatic continuity equation. The parameter ε is the central point of attention for non-hydrostatic dynamics. In meso- and large-scale atmospheric flows, $\varepsilon << 1$.

Discretization of equations

The discretization of model equations is as follows.

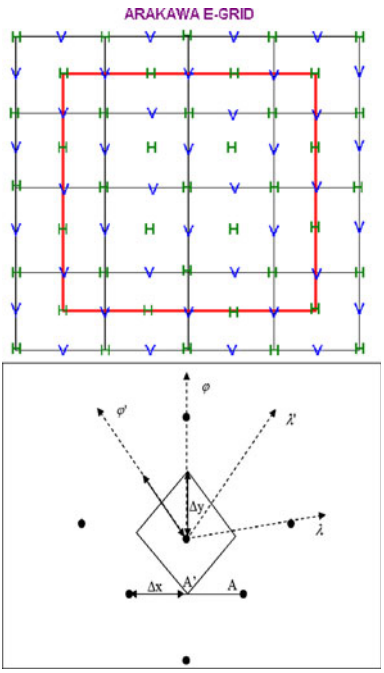

Horizontal discretization equation

In order to organize the spurious accumulation of energy at the smallest resolvable scales, an energy and enstrophy conserving advection scheme for the semi-staggered E-grid is used (Arakawa and Lamb 1977).

The horizontal advection scheme for the E-grid is defined by,

$$\begin{aligned} U &= \overline{\Delta\pi}^{\lambda} u 2\Delta x \\ V &= \overline{\Delta\pi}^{\varphi} v 2\Delta y \\ U' &= \overline{\Delta\pi}^{\lambda'} \left(\overline{u\Delta y + v\Delta x}^{\varphi'} \right) \\ V' &= \overline{\Delta\pi}^{\varphi'} \left(\overline{-u\Delta y + v\Delta x}^{\lambda'} \right) \\ A &= 4\Delta x\Delta y, A' = 2\Delta x\Delta y \end{aligned}$$

where $\Delta\pi$ is the thickness of the layer in hydrostatic pressure and $\Delta x = a\cos(\varphi)\Delta\lambda, \Delta y = a\Delta\varphi$. Then the horizontal advection for T, u and v are defined as,

$$\begin{aligned} \frac{\partial T}{\partial t} &= -\frac{1}{\Delta\pi}\left[\frac{1}{3}\frac{1}{A}\left(\overline{U\Delta_\lambda T}^{\lambda} + \overline{V\Delta_\varphi T}^{\varphi}\right) + \frac{2}{3}\frac{1}{A'}\left(\overline{U'\Delta_{\lambda'} T}^{\lambda'} + V\Delta_\varphi T^{\varphi'}\right)\right] + \cdots \\ \frac{\partial u}{\partial t} &= -\frac{1}{\overline{\Delta\pi}^{\lambda}}\left[\frac{1}{3}\frac{1}{A}\left(\overline{U^{\lambda}\Delta_\lambda u}^{\lambda} + \overline{V^{\lambda}\Delta_\varphi u}^{\varphi}\right) + \frac{2}{3}\frac{1}{A'}\left(\overline{U'^{\lambda}\Delta_{\lambda'} u}^{\lambda'} + \overline{V'^{\lambda}\Delta_{\varphi'} u}^{\varphi'}\right)\right] + \cdots \\ \frac{\partial v}{\partial t} &= -\frac{1}{\overline{\Delta\pi}^{\varphi}}\left[\frac{1}{3}\frac{1}{A}\left(\overline{U^{\varphi}\Delta_\lambda v}^{\lambda} + \overline{V^{\varphi}\Delta_\varphi v}^{\varphi}\right) + \frac{2}{3}\frac{1}{A'}\left(\overline{U'^{\varphi}\Delta_{\lambda'} v}^{\lambda'} + \overline{V'^{\varphi}\Delta_{\varphi'} v}^{\varphi'}\right)\right] + \cdots \end{aligned}$$

In horizontal co-ordinate system, in order to achieve higher computational efficiency of the model code, a transformed latitude-longitude coordinate system is used. This system is obtained by rotation of the natural geodesic latitude-longitude in such a way that the intersection of the equator and zero meridian of the transformed system (λ_0, φ_0) coincides with the center of the model domain. The transformation and inverse transformation equations between the rotated and the natural latitude-longitude system (λ, φ) are as follows.

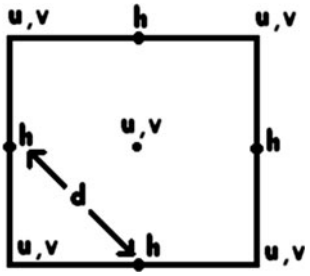

$$\begin{aligned} \Lambda &= \arctan\frac{\cos\varphi\sin(\lambda-\lambda_0)}{\cos\varphi_0\cos\varphi\cos(\lambda-\lambda_0)+\sin\varphi_0\sin\varphi} \\ \Phi &= \arcsin(\cos\varphi_0\sin\varphi - \sin\varphi_0\cos\varphi\cos(\lambda-\lambda_0)) \\ \varphi &= \arcsin(\sin\varphi_0\cos\Phi\cos\Lambda + \cos\varphi_0\sin\Phi \\ \lambda &= \lambda_0 + \arcsin\left(\frac{\sin\Lambda\cos\Phi}{\cos\varphi_0}\right) \end{aligned}$$

The horizontal wind in the rotated system $\mathbf{V} = (U, V)$ expressed in terms of the wind in the natural latitude/longitude system $\mathbf{v} = (u,v)$ is defined as;

$$U = \frac{u[\cos\varphi_0\cos\varphi + \sin\varphi_0\sin\varphi\cos(\lambda-\lambda_0)] - v\sin\varphi_0\sin(\lambda-\lambda_0)}{\sqrt{1-[\cos\varphi_0\sin\varphi - \sin\varphi_0\cos\varphi\cos(\lambda-\lambda_0)]^2}}$$

$$V = \frac{u\sin\varphi_0\sin(\lambda-\lambda_0) + v[\cos\varphi_0\cos\varphi + \sin\varphi_0\sin\varphi\cos(\lambda-\lambda_0)]}{\sqrt{1-[\cos\varphi_0\sin\varphi - \sin\varphi_0\cos\varphi\cos(\lambda-\lambda_0)]}}$$

The inverse wind transformation is given by,

$$u = \frac{U(\cos\varphi_0\cos\Phi - \sin\varphi_0\sin\Phi\cos\Lambda) + V\sin\varphi_0\sin\Lambda}{\sqrt{1-(\cos\varphi_0\sin\Phi + \sin\varphi_0\cos\Lambda\cos\Phi)^2}}$$

$$v = \frac{-U\sin\varphi_0\sin\Lambda + V(\cos\varphi_0\cos\Phi - \sin\varphi_0\sin\Phi\cos\Lambda}{\sqrt{1-(\cos\varphi_0\sin\Phi + \sin\varphi_0\cos\Lambda\cos\Phi)^2}}$$

Vertical discretization equations

The Lorenz vertical staggering of the variables is used in the vertical (Janjic 1977). The geopotential and non-hydrostatic pressure are defined at the interfaces of the layers, while all three velocity components and temperature are carried in the middle layers of the model. The vertical velocity is defined at the E-grid mass points.

The terrain following hydrostatic-pressure-based sigma coordinate up to a specified pressure surface usually below the tropopause, and hydrostatic pressure coordinate above. Top of the model is constant pressure surface.

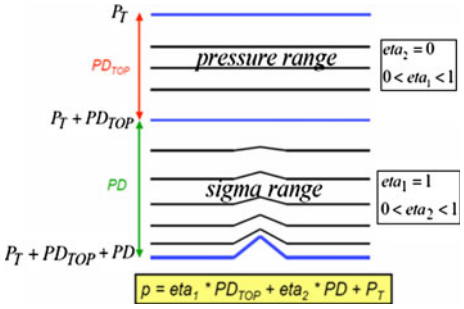

In the pressure range,

$$\nabla_p \cdot (\mathbf{v}) + \frac{\partial\omega}{\partial p} = 0$$

In the sigma range,

$$\frac{\partial PD}{\partial t} + \nabla_\sigma \cdot (PD\,\mathbf{v}) + \frac{\partial(PD\dot{\sigma})}{\partial\sigma} = 0$$

where as $PD\dot{\sigma} = \omega$ at the vertical level of the model where sigma range changes to the pressure range.

Hence, the mass continuity equation can be written as:

For the pressure range:

$$0 = -\left[\frac{1}{3}\frac{1}{A}\left(\Delta_\lambda U + \Delta_\varphi V\right) + \frac{2}{3}\frac{1}{A'}\left(\Delta_{\lambda'} U' + \Delta_{\varphi'} V'\right)\right] - \Delta_\pi \omega$$

For the sigma range:

$$\frac{\partial \Delta\pi}{\partial t} = -\left[\frac{1}{3}\frac{1}{A}\left(\Delta_\lambda U + \Delta_\varphi V\right) + \frac{2}{3}\frac{1}{A'}\left(\Delta_{\lambda'} U' + \Delta_{\varphi'} V'\right)\right] - \Delta_\sigma(\mu\dot{\sigma})$$

For the interface between sigma and pressure range:

$$(\mu\dot{\sigma})_I = \omega_I$$

Time discretization equations

HWRF uses four types of time integration: (i) modified Adams–Bashforth scheme for horizontal advection of u, v and T, and Coriolis terms, (ii) Crank–Nicholson for vertical advection of u, v and T, (iii) forward–backward scheme for adjustment terms and (iv) an implicit scheme for vertically propagating sound waves.

The Adam-Bashforth scheme can be represented as:

$$\frac{y^{\tau+1} - y^{\tau}}{\Delta t} = \frac{3}{2} f(y^{\tau}) - \frac{1}{2} f\left(y^{\tau-1}\right)$$

This method has a slight linear instability, which can be stabilized as;

$$\frac{y^{\tau+1} - y^{\tau}}{\Delta t} = 1.533 f(y^{\tau}) - 0.533 f\left(y^{\tau-1}\right)$$

The Crank–Nicholson scheme can be represented as:

$$\frac{y^{\tau+1} - y^{\tau}}{\Delta t} = \frac{1}{2}\left[f\left(y^{\tau+1}\right) + f(y^{\tau})\right]$$

This is an implicit scheme and so is always stable.

The time integration for the terms involving the propagation of gravity waves is handled by a forward–backward process.

Using the shallow water equation,

$$\frac{\partial u}{\partial t} = -g\frac{\partial h}{\partial x}, \quad \frac{\partial h}{\partial t} = -H\frac{\partial u}{\partial x}$$

The mass tendency equation is advanced by a forward step:

$$h^{\tau+1} = h^{\tau} - \Delta t\, H\, \frac{\partial u^{\tau}}{\partial x}$$

The velocity equations are then advanced with a backward step:

$$u^{\tau+1} = u^{\tau} - \Delta t\, g\, \frac{\partial h^{\tau+1}}{\partial x}$$

The time integration for vertically propagating sound waves is:

$$\frac{\partial^2 p'}{\partial t^2} = \frac{p'^{n+1} - 2p'^{n} + p'^{n-1}}{\Delta t^2} = \frac{\mathbf{c}_p}{\mathbf{c}_v} R\, T_0\, \frac{\partial^2 p'^{n+1}}{\partial z_0^2},$$

where p' represents a perturbation pressure

The advection of other variables such as water vapor and liquid water uses the Langangian forward time differencing, which can be represented as:

$$\frac{y_j^{\tau+1*} - y_j^{\tau}}{\Delta t} = -u\frac{y_j^{\tau} - y_{j-1}^{\tau}}{\Delta x}, \quad u > 0$$

This is followed by a negative diffusion step to reduce smoothing:

$$\frac{y_j^{\tau+1} - y_j^{\tau+1*}}{\Delta t} = -f\left(\frac{u\Delta t}{\Delta x}\right)\frac{y_{j-1}^{\tau+1*} - 2y_j^{\tau+1*} + y_{j+1}^{\tau+1*}}{\Delta x}, \quad f\left(\frac{u\Delta t}{\Delta x}\right) > 0$$

With the non-hydrostatic approach, with vanishing ε, the time discrete equation with adding Crank–Nicholson vertical and Adams–Bashforth horizontal advection can be written as:

$$T_1^* = T^n - \Delta t\left(\mathbf{v}^n \cdot \nabla_\sigma T^{n+1/2} + \dot{\sigma}^n \frac{\partial T^{n+1/2}}{\partial \sigma}\right)$$

Finally

$$T_1 = T_1^* + \frac{\Delta t}{\mathbf{c}_p}\frac{RT^n}{p^n}\omega_1$$

Lateral boundary condition

The velocity and mass variables are specified only on the outermost rows and columns. On the first row or column from the outer boundaries, each variable is replaced by a four point average from its surrounding points (Mesinger and Janjic 1974, Mesinger 1977). Inside the domain, the initial values before the averaging are defined by the tendency equations with the advection terms computed using upstream differences on the three rows next to the internal boundary where the four-point averaging is applied. The enhanced divergence damping is generally applied close to the boundaries.

The vertical boundary conditions are:

$$\dot{\sigma} = 0 \quad \text{and} \quad p - \pi = 0 \text{ at } \sigma = 0$$

and

$$\dot{\sigma} = 0 \quad \text{and} \quad \frac{\partial(p - \pi)}{\partial \sigma} = 0 \text{ at } \sigma = 1$$

References

Arakawa A, Lamb VR (1977) Computational design of the basic dynamical processes of the UCLA general circulation model. In: Chang J (ed) Methods in computational physics, vol 17. Academic Press, pp 173–265

Arakawa A, Schubert WH (1974) Interaction of a cumulus cloud ensemble with the large scale environment. Part I. J Atmos Sci 31:674–701

Bao J-W, Wilczak JM, Chio J-K, Kantha LH (2000) Numerical simulation of air–seas interaction under high wind conditions using a coupled model: a study of hurricane development. Mon Weather Rev 128:2190–2210

Black TL (1994) The new NMC mesoscale Eta model: description and forecast examples. Weather Forecast 9:265–278

Braun SA, Tao W-K (2000) Sensitivity of high-resolution simulations of hurricane Bob (1991) to planetary boundary layer parameterizations. Mon Weather Rev 128:3941–3961

Dudhia J (1993) A non-hydrostatic version of Penn State–NCAR mesoscale model: validation tests and simulation of an Atlantic cyclone and cold front. Mon Weather Rev 121:1493–1513

Fels SB, Schwarzkopf MD (1975) The simplified exchange approximation: a new method for radiative transfer calculation. J Atmos Sci 32:1475–1488

Gopalakrishnan SG, Bacon DP, Ahmad NN, Boybeyi Z, Dunn TJ, Hall MS, Jin Y, Lee PCS, Madala RV, Ananthakrishna Sarma R, Turner MD, Wait T (2002) An operational multi-scale atmospheric model with grid adaptivity for hurricane forecasting. Mon Wea Rev 130(7):1830–1847

Grell GA (1993) Prognostic evaluation of assumptions used by cumulus parameterizations. Mon Wea Rev 121:764–787

Hong S–Y, Pan H–L (1996) Non-local boundary layer vertical diffusion in a medium-range forecast model. Mon Wea Rev 124:2322–2339

IMD (June 2007) Tracks of cyclones and depressions in the Bay of Bengal and Arabian Sea during 2006

Janjic ZI (1977) Pressure gradient force and advection scheme used for forecasting with steep and small scale topography. Contrib Atmos Phy 50:186–199

Janjic ZI (1984) Non-linear advection schemes and energy cascade on semi-staggered grids. Mon Wea Rev 112:1234–1245

Janjic ZI (2003) A non-hydrostatic model based on a new approach. Met Atmos Phy 82:271–285

Janjic ZI, Gerrity JP Jr, Nickovic S (2001) An alternative approach to non-hydrostatic modeling. Mon Wea Rev 129:1164–1178

Lacis AA, Hansen JE (1974) A parameterization for the absorption of solar radiation in the earth's atmosphere. J Atmos Sci 31:118–133

Liu Y, Zhang D–L, Yau MK (1997) A multi-scale numerical simulation of hurricane Andrew (1992). Part-I: explicit simulation and verification. Mon Wea Rev 125:3073–3093

Liu Y, Zhang D–L, Yau MK (1999) A multi-scale numerical simulation of hurricane Andrew (1992). Part-II: kinematics and inner core structure. Mon Wea Rev 127:2597–2616

Majumdar AB, Lele RR, Sunitha Devi S (2007) Cyclones and depressions over NIO during 2006. Mausam 58(3):303–322

Mandal M, Mohanty UC, Sinha P, Ali MM (2007) Impact of sea surface temperature in modulating movement and intensity of tropical cyclones. Natural Hazard 41:413–427

Mesinger F (1977) Forward-backward scheme, and its use in a limited area model. Contrib Atmos Phys 50:200–210

Mesinger F, Janjic ZI (1974) Noise due to time-dependent boundary conditions in limited area models. The GARP Programme on Numerical Experimentation, Rep No 4, WMO, Geneva, pp 31–32

Mohanty UC (1994) Tropical cyclones in the Bay of Bengal and deterministic methods for prediction of their trajectories. Sadhana 19(4):567–582

Mohanty UC, Gupta A (1997) Deterministic methods for prediction of tropical cyclone tracks. Mausam 48(2):257–272

Mohanty UC, Mandal M, Raman S (2004) Simulation of Orissa super cyclone (1999) using PSU/NCAR mesoscale model. Nat Hazards 31(2):373–390

Mohanty UC, Pattanayak S, Osuri KK (2010) Changes in frequency and intensity of tropical cyclones over Indian seas in a warming environment. Disaster Dev 4:53–77

Pattanayak S, Mohanty UC (2008) A comparative study on performance of MM5 and WRF models in simulation of tropical cyclones over Indian seas. Curr Sci 95(7):923–936

Schwarzkopf MD, Fels SB (1985) Improvements to the algorithm for computing CO2 transmissivities and cooling rates. J Geophys Res 90:541–550

Schwarzkopf MD, Fels SB (1991) The simplified exchange method revisited: an accurate, rapid method for computations of infrared cooling rates and fluxes. J Geophys Res 96:9075–9096

Skamarock WC, Klemp JB, Dudhia J, Gill DO, Barker DM, Wang W, Powers JG (2005) A description of the advanced research WRF version 2

Wong KY, Yip CL (2005a) Tropical cyclone eye fix using genetic algorithm with temporal information. In: Proceedings of the 9th international conference on knowledge-based intelligent information and engineering systems (KES-2005). LNAI, Melbourne, Australia, pp 854–860

Wong KY, Yip CL (2005b) An intelligent tropical cyclone eye fix system using motion field analysis. In: Proceeding of the 17th IEEE international conference on tools with artificial intelligence (ICTAI-2005). Hong Kong, pp 652–656

Xue M, Droegemeier KK, Wong V (2000) The advanced regional prediction system (ARPS)—a multiscale nonhydrostatic atmospheric simulation and prediction tool. Part I: model dynamics and verification. Meteor Atmos Phys 75:161–193

Xue M, Droegemeier KK, Wong V, Shapiro A, Brewster K, Carr F, Weber D, Liu Y, Wang D-H (2001) The advanced regional prediction system (ARPS)—a multiscale nonhydrostatic atmospheric simulation and prediction tool. Part II: model physics and applications. Meteor Atmos Phys 76:134–165

Zhang D–L, Wang X (2003) Dependence of hurricane intensity and structure on vertical resolution and time-size. Adv Atmos Sci 20:711–725